Applied Catalysis B: Environmental 150–151 (2014) 1–11

Contents lists available at ScienceDirect

Applied Catalysis B: Environmental

journal homepage: www.elsevier.com/locate/apcatb

Ferrous ions promoted aerobic simazine degradation with Fe@Fe_2O_3 core–shell nanowires

Wei Liu, Zhihui Ai, Menghua Cao, Lizhi Zhang*

Key Laboratory of Pesticide & Chemical Biology of Ministry of Education, Institute of Environmental Chemistry, College of Chemistry, Central China Normal University, Wuhan 430079, People's Republic of China

ARTICLE INFO

Article history:
Received 26 October 2013
Received in revised form
16 November 2013
Accepted 21 November 2013
Available online 28 November 2013

Keywords:
Fe@Fe_2O_3 nanowires
Molecular oxygen activation
Surface bound ferrous ions
Surface hydroxyl radicals
Simazine

ABSTRACT

In this study, we investigated the effect of extra ferrous ions on the aerobic simazine degradation with Fe@Fe_2O_3 core–shell nanowires at circumneutral pH and interestingly found that ferrous ions could promote the aerobic simazine degradation efficiency of nanowires by about 5 times. The aerobic simazine degradation improvement was realized by maintaining enough dissolved ferrous ions and enhancing single-electron reduction molecular oxygen activation via providing more surface bound ferrous ions on the iron oxide shell. These increased surface bound ferrous ions could produce more surface hydroxyl radicals to enhance the simazine degradation. The 2,2′-bipytridine inhibition and reactive oxygen species detection results revealed that the contribution of sequential single-electron molecular oxygen activation by surface bound ferrous ions to reactive oxygen species production was more than 60%, higher than that of two-electron molecular oxygen activation pathway. We determined the degradation intermediates of simazine with high performance liquid chromatography–mass spectrometry and gas chromatography–mass spectrometry to tentatively propose a possible simazine degradation pathway. These interesting findings could provide new insight on nanoscale zero valent iron induced molecular oxygen activation and its aerobic removal of organic pollutants at circumneutral pH.

1. Introduction

Simazine is one of the most common chloro-*s*-triazine herbicides and widely used to inhibit the growth of broad-leaf weeds and annual grassy in crop fields [1]. However, it is believed to pose adverse effects on algal flora in soil and water because of its estrogenic effect on various cell lines, and also regarded as a possible endocrine disrupter and human carcinogen [2,3]. Because of its moderate persistent in the soil (average field half-life of 60 days) and extensive use, simazine has been found in rivers, ground waters, soils, and even rainfall [4–7]. Therefore, it is of great importance to remove widespread simazine existed in the environment. Although there are many methods for the simazine removal, including sorption [8], Fenton's oxidation [9], photocatalytic oxidation [10], ozonation [11], and biological methods [12], most of these methods involve the utilization of some expensive reagents and/or are time consuming. Thus it is still a challenge to develop more efficient and low cost method for the control and remediation of simazine pollution.

Iron is one of the most abundant transition metal elements in the Earth's crust [13]. The conversion between Fe^{3+} and Fe^{2+} (iron cycle) participates in many important environmental and biochemical processes, including the generation and consumption of reactive oxygen species (ROSs), the decomposition and conversion of organics, as well as the respiration and nutrition intake of some microorganism, etc. Molecular oxygen in air is thought to be the most green and low cost oxidant. Unfortunately, molecular oxygen could not oxidize most of organic pollutants under ambient conditions because of spin forbidden reactions [14,15]. Therefore, the molecular oxygen activation with low-valent iron (Fe^0 and Fe^{2+}) would be highly desirable for organic pollutant control and remediation in view of economical and environmental points. For example, nano zero-valent iron (nZVI) could activate molecular oxygen to produce various ROSs for the oxidative removal of chlorinated phenols, molinate, arsenic(III), and so on [16–20].

Fe@Fe_2O_3 core–shell nanowires are a special kind of nZVI developed by our group and can be used as an effective heterogeneous Fenton iron reagent to degrade dye and pentachlorophenol, and dimethyl phthalate [21–27], as well as a reductant/adsorbent to efficiently remove Cr(VI) [28]. Recently, we reported the core–shell structure dependent reactivity of Fe@Fe_2O_3 nanowires on the aerobic degradation of 4-chlorophenol and proposed a new nZVI induced molecular oxygen activation mechanism to explain this interesting structure dependent reactivity. The molecular oxygen activation mechanism combined a two-electron molecular oxygen activation pathway via the outward electron transfer from iron core

* Corresponding author. Tel.: +86 27 6786 7535; fax: +86 27 6786 7535.
E-mail address: zhanglz@mail.ccnu.edu.cn (L. Zhang).

0926-3373/$ – see front matter © 2013 Elsevier B.V. All rights reserved.
http://dx.doi.org/10.1016/j.apcatb.2013.11.034

to the iron oxide shell surface and a single-electron molecular oxygen activation process by surface bound ferrous ions on the iron oxide shell [29]. However, the contributions of these two pathways on the ROSs production are not clear yet. In this study, we systematically investigate the effect of extra ferrous ions on the aerobic simazine degradation with Fe@Fe_2O_3 nanowires and the generation of ROSs. 2,2′-bipytridine is used to inhibit the single-electron molecular oxygen activation pathway to estimate its contribution to the ROSs production. Liquid chromatography–mass spectrometry and gas chromatography–mass spectrometry are used to determine the intermediates of simazine degradation to clarify the simazine degradation mechanism.

2. Experimental

2.1. Chemicals and materials

$FeCl_3{\cdot}6H_2O$, $FeSO_4{\cdot}7H_2O$, KI, C_2H_5OH, $NaBH_4$, and 2,2′-bipytridine were all of analytical grade and purchased from National Medicines Corporation Ltd. of China. Simazine (≥99.9%) was purchased from Supelco. superoxide dismutase (SOD), catalase (CAT), horseradish peroxidase, and *p*-hydroxyphenylacetic acid (POHPAA) were purchased from Sigma-Aldrich (St. Louis, MO). Two buffers of sodium acetate (pH 5.0) and piperazine-*N*,*N*′-bis (ethanesulfonic acid) (PIPES; pH 7.0) were prepared with the reagents of analytical grade purchased from National Medicines Corporation Ltd. of China. High performance liquid chromatography (HPLC) grade methanol, iso-propanol and acetonitrile were obtained from Fisher Scientific. Fe@Fe_2O_3 core–shell nanowires were synthesized by the reduction of ferric ions with sodium borohydride without any stirring [21]. All the chemicals were used as received without further purification. Argon (Ar, ≥99.9%) gas and a mixture gas of 3% H_2 and 97% Ar were supplied by Hubei Minghui Gas Company, China. De-ionized water was used throughout the experiments.

2.2. Experimental procedure

The stock solution of simazine was prepared by dissolving simazine in deionized water and stored in dark to avoid any photochemical degradation. All the degradation experiments were conducted in 25 mL conical flasks. The reaction suspension was prepared by adding 0.1120 g of Fe@Fe_2O_3 into 20 mL of 0.025 mmol/L (5 mg/L) simazine solution without pH adjusting. Different amounts of $FeSO_4{\cdot}7H_2O$ were added to the solution to investigate the influence of extra ferrous ions on the oxidative degradation of simazine. Each flask was sealed with Teflon-lined cap and then incubated at room temperature. Control experiments were conducted by using the same procedures with certain amounts of Fe@Fe_2O_3 or $FeSO_4{\cdot}7H_2O$, respectively. Air or argon was pumped into the solution at a rate of 1.5 L/min to continuously supply molecular oxygen or remove molecular oxygen, respectively. 0.5 mL of sample aliquot was withdrawn at a regular time interval from the flask with a syringe and passed through a 0.22 μm polytetrafluoroethylene filter for further analysis. The concentration of simazine was analyzed by HPLC at an interval time of 1 h. The initial pH values of the simazine solutions were adjusted with NaOH and hydrochloric acid of 1 mol/L concentrations. All of the degradation experiments were replicated for three times.

The simazine removal processes with different scavengers were carried out by adding excess SOD, CAT and iso-propanol. 10 mmol/L of KI was also used to probe the generation of hydroxyl radicals on the surface of the catalysts. 20 mmol/L of 2,2′-bipytridine (BPY) was used to complex the ferrous ions to prevent its oxidation with hydrogen peroxide or oxygen. All others parameters were the same as the degradation processes.

2.3. The hydrogen reduction of Fe@Fe_2O_3 core–shell nanowires

The reduction of as-prepared Fe@Fe_2O_3 was conducted with using a conventional two-zone horizontal tube furnace (OTF-1200X, China). The temperature of the furnace was gradually increased from the room temperature to the growth temperature (400 °C) at a rate of 10 °C/min. After maintaining that temperature for 1 h, the furnace was allowed to cool naturally to room temperature by switching off the heating power. All of the processes were carried out with a mixture gas of 3% H_2 and 97% Ar.

2.4. Analytic methods

The dissolved ferrous ions was quantified by the 1,10-phenanthrolin method [30], and the total dissolved iron ions was quantified after adding hydroxylamine hydrochloride to the filtered solution. Samples were analyzed by a UV–vis spectrophotometer (UV-2550, Shimadzu, Japan) at maximum wavelength of 510 nm.

Hydrogen peroxide was measured using a modified horseradish peroxidase-mediated dimerization of POHPAA method [31]. First, a certain volume of fluorescence reagent (potassium hydrogen phthalate: 8.2 g/L, *p*-hydroxyphenylacetic acid: 270 mg/L, and type II horseradish peroxidase: 30 mg/L) was pre-added into the reaction system. 1.0 mL of sample was then withdrawn at an interval time of 2 h and then mixed with 1.0 mL of 1.0 mol/L NaOH for 10 min for measuring the intensity of the fluorescence peak emission peak at 400 nm when excited at 320 nm.

Terephthalic acid was used as the probe for the ·OH detection. The reaction of terephthalic acid with hydroxyl radicals could produce 2-OH-terephthalic acid with a fluorescence peak located at 426 nm after excitation at 312 nm. We measured the fluorescence intensity of the generated 2-OH-terephthalic acid with a FluoroMax-P spectrophotometer.

The concentration of simazine was analyzed by high pressure liquid chromatography (HPLC, LC-20A, Shimadzu, Japan), which equipped with an automatic injector model SIL-20A, LC-20AT pump, and a SPD-M20A photodiode array detector. The temperature of column was maintained at 30 °C by a CTO-20AS oven. A ZORBAX SB-C18 (5 μm, 4.6 × 150 mm; Agilent, USA) column was used in the analysis. The maximum absorption wavelength (λ_{max}) of simazine was determined and selected as 220 nm. A mixture of 50% water and 50% acetonitrile was used as the mobile phase running at a flow rate of 1.0 mL/min. The injective volume was 10 μL.

Identification of intermediates was conducted by liquid chromatography–mass spectrometry (LC–MS) at positive modes and MS/MS analysis, utilizing a triple quadrupole mass spectrometer (API2000, ABI, USA) equipped with an ESI interface. The chromatography was performed on a ZORBAX SB-C18 (5 μm, 4.6 × 250 mm; Agilent, USA) column, the mobile phase was acetonitrile/water (10/90, v/v) in the first 3 min. The content of acetonitrile in the mobile phase increased to 50% at 25 min and continued for 2.5 min, then decreased to 10% and continued for 12.5 min. The total analysis time was 40 min. The flow rate was set at 1.0 mL/min and the injection voltage was 10 μL. The MS capillary temperature was set at 250 °C with a voltage of 46 V and a spray voltage of 4.5 kV. The MS/MS tests were carried out using helium as the collision gas (30% and 100% collision energy corresponding to 5 V from peak to peak).

The intermediates were also detected by gas chromatography mass spectrometry (GC–MS TRACE 1300-ISQ; Thermo). A HP-5MS column (30 m × 0.25 mm × 0.25 μm) was employed for separation and analysis of reaction products. The inlet temperature was 280 °C, and the detector temperature was 320 °C. The oven temperature was initiated at 50 °C and held for 3 min, and then increased to 200 °C at 10 °C/min and held for 10 min, after that the temperature was increased to 270 °C at 20 °C/min and held for 5 min. The flow

rate of the carrier gas helium was 1.0 mL/min. The injection of 1 μL sample was conducted by an AI 1310 autosampler in the pulsed splitless mode and the split mode was turned on after 1.0 min. The temperatures of transfer line, ion source, and MS detector were 280, 230 and 150 °C, respectively. The MS detector was operated in the electron impact mode with 70 eV of ionization energy and the mass spectra were acquired in the full scan mode with m/z ranging from 50 to 1000.

2.5. Characterizations

X-ray diffraction (XRD) patterns were obtained on a Bruker D8 Advance X-ray diffractometer with Cu Ka radiation. Scanning electron microscopy (SEM) was performed on a LEO 1450VP scanning electron microscope.

3. Results and discussion

The aerobic degradation of simazine with Fe@Fe_2O_3 nanowires was evaluated in the absence (Fe@Fe_2O_3/air) or presence (Fe(II)/Fe@Fe_2O_3/air) of ferrous ions at room temperature. For comparison, the simazine degradation was also carried out in the presence of ferrous ions and air without adding Fe@Fe_2O_3 nanowires (Fe(II)/air). It was found that ferrous ions alone could not induce the degradation of simazine in air, while Fe@Fe_2O_3 could aerobically degrade 60% of simazine within 8 h (Fig. 1a). Interestingly, the aerobic simazine removal efficiency in 8 h could reach 97% in the Fe(II)/Fe@Fe_2O_3/air system. Both of the aerobic simazine removal curves over Fe@Fe_2O_3 and Fe(II)/Fe@Fe_2O_3 were found to fit pseudo-first-order kinetics equations. The apparent simazine degradation constant (0.5009 h^{-1}) over Fe(II)/Fe@Fe_2O_3 was about 5 times that (0.1039 h^{-1}) over Fe@Fe_2O_3 as shown in Fig. 1b.

As the addition of ferrous ions changed the pH value of the solution, which would further affect the rate of the reaction between the ferrous ions and oxygen, we monitored the pH value changes during the aerobic simazine degradation in the Fe(II)/air, Fe@Fe_2O_3/air, and Fe(II)/Fe@Fe_2O_3/air systems (Fig. 2a). The pH value of the Fe@Fe_2O_3/air system decreased from 8.5 to 6.8, while the pH values of the Fe(II)/air and Fe(II)/Fe@Fe_2O_3/air systems decreased respectively from 6.0 to 4.8 and 6.5 to 5.0, revealing that the addition of ferrous ions resulted in a pH drift of about 2. Regarding all the pH values fluctuated between 4.8 and 8.5, we thus compared the simazine removal efficiencies of Fe(II)/air, Fe@Fe_2O_3/air, Fe(II)Fe@Fe_2O_3/air system at initial pH values of 5 and 8 after pH adjusting with NaOH and hydrochloric acid, and found that the initial pH changes did not affect the aerobic simazine degradation (Fig. 2b and c). Meanwhile, we also noticed that the pH increased from 5.0 to about 6.5 in the first 2 h and maintained at 6.5 later in case of the initial pH of 5.0 during the aerobic simazine degradation (Fig. 3a). This pH increase could be attributed to the proton consumption by the corrosion of Fe^0 core and/or the generation of hydrogen peroxide. To further check the influence of pH on the simazine degradation in the Fe@Fe_2O_3/air and Fe(II)/Fe@Fe_2O_3/air systems, we therefore employed two common buffer solutions of PIPES (pH = 7.0) and sodium acetate (pH = 5.0) to maintain the pH unchanged during the simazine degradation in the two systems (Fig. 3b). Surprisingly, the utilization of two buffer solutions completely inhibited the aerobic degradation of simazine, revealing the presence of buffer solution affected the aerobic simazine degradation over Fe@Fe_2O_3 no matter whether ferrous ions were added or not. We subsequently selected 4-chlorophenol as the target pollutant to compare the removal efficiencies of Fe@Fe_2O_3 and Fe(II)/Fe@Fe_2O_3 systems in the two buffer solutions (Fig. 3c), and found that 4-chlorophenol could be degraded at pH 5.0, but not at pH 7.0. More importantly, the removal efficiency (60% in 4 h) of the Fe(II)/Fe@Fe_2O_3/air system was significantly higher than that (30% in 4 h) in the Fe@Fe_2O_3/air system when the sodium acetate buffer solution (pH 5.0) was employed for both of the two systems. So we conclude that the addition of ferrous ions could significantly promote the aerobic simazine degradation because of the interaction between the ferrous ions and the Fe@Fe_2O_3 nanowires, rather than the molecular oxygen activation by the dissolved ferrous ions and the simply shift of the oxidants from ferryl ions to hydroxyl radicals by the effect of the pH drift [16,20].

The effects of extra ferrous ions on the aerobic degradation of simazine were then investigated in the presence of different concentrations (0, 1, 3, 5 mmol/L) of ferrous ions (Table 1). All the

Table 1
Pseudo-first-order constants, the corresponding coefficients, and residual simazine after 8 h of degradation in the Fe@Fe_2O_3/air system with adding different dosage of ferrous ions.

$c_{Fe(II)}$ (mmol/L)	Degradation constant (h^{-1})	Coefficient (R^2)	Residual simazine (%)
0	0.1039	0.8661	41
1	0.1998	0.9593	23
3	0.5009	0.9698	3
5	0.3218	0.9572	10

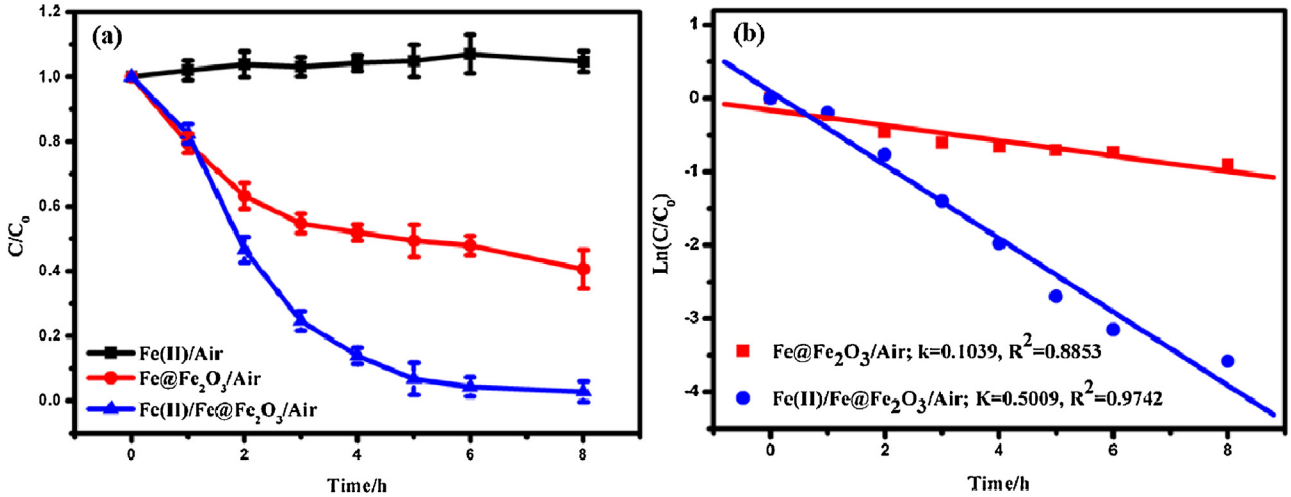

Fig. 1. (a) The aerobic removal curves of simazine in Fe(II)/air, Fe@Fe_2O_3/air and Fe(II)/Fe@Fe_2O_3/air systems; (b) plots of ln(C/C_0) versus time for the aerobic removal of simazine in Fe@Fe_2O_3/air and Fe(II)/Fe@Fe_2O_3/air systems.

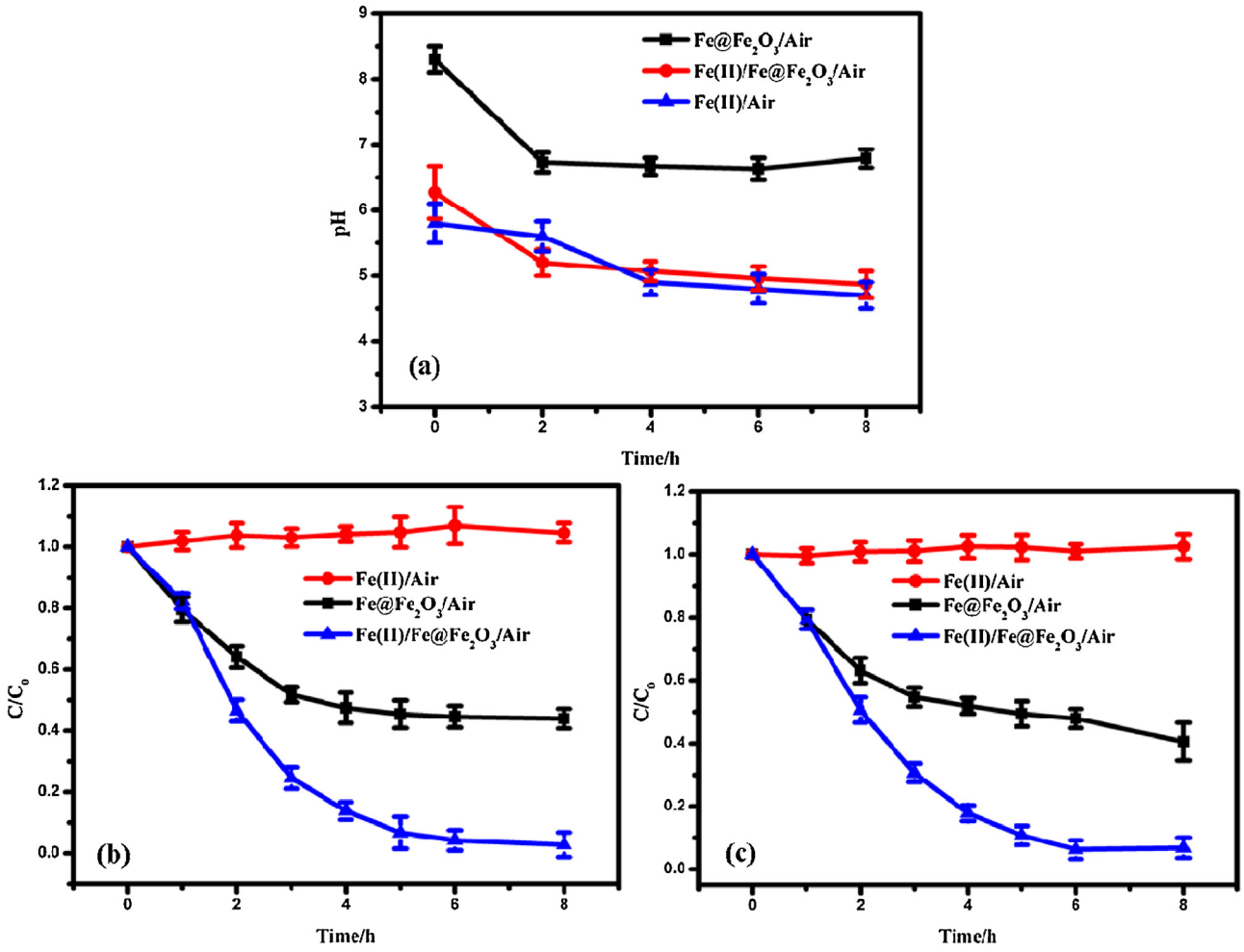

Fig. 2. (a) The changes of the pH value during the simazine removal in the Fe(II)/air, Fe@Fe_2O_3/air and Fe(II)/Fe@Fe_2O_3/air systems; (b) the aerobic removal of simazine with different systems at initial pH of 5; and (c) the aerobic removal of simazine with different systems at initial pH of 8.

simazine removal efficiencies in the presence of ferrous ions were higher than that in the absence of ferrous ions. Furthermore, the removal efficiency increased with the concentration of ferrous ions from 1 to 3 mmol/L, and then decreased significantly when the concentration of ferrous ions increased to 5 mmol/L. Therefore, the ferrous ions dosage of 3 mmol/L was used for the following experiments. Subsequently, we monitored the concentration changes of dissolved ferrous, ferric and total iron ions during the aerobic simazine degradation in the Fe@Fe_2O_3/air and Fe(II)/Fe@Fe_2O_3/air systems. As for the Fe@Fe_2O_3/air system (Fig. 4a), ferrous ions were immediately generated as soon as Fe@Fe_2O_3 was added into the aqueous simazine solution. The concentration of dissolved ferrous ions increased to a maximum value of 0.055 mmol/L in the first 1 h, and then decreased quickly and finally approached to 0 mmol/L after 5 h, which might be caused by the consumption of ferrous ions through Fenton reaction. The dissolved ferrous ions concentration change curve matched well with the aerobic simazine degradation curve over Fe@Fe_2O_3 shown in Fig. 1a. Interestingly, the concentration of ferrous ions continuously increased during the simazine degradation process in the Fe(II)/Fe@Fe_2O_3/air system (Fig. 4b), it revealed that the addition of ferrous ions could maintain enough dissolved ferrous ions. This is because these added ferrous ions themselves could not only increase the amount of dissolved ferrous ions, but also lower pH to release more ferrous ions from Fe@Fe_2O_3 nanowires in the Fe(II)/Fe@Fe_2O_3/air system. However, the concentrations of dissolved ferric ions in both of two systems were very low, suggesting the reduction of ferric ions by the Fe^0 core and/or the conversion of ferric ions into iron oxide/hydroxide because ferric ions are sparingly soluble.

X-ray diffraction (XRD) analysis and scanning electron microscopy (SEM) were used to probe the phase and morphology changes of Fe@Fe_2O_3 nanowires in the presence or absence of ferrous ions during the aerobic simazine removal (Figs. 5 and 6). The diffraction peak at 2θ value of 44.9° being attributed to the metallic Fe (JCPDS, file no. 87-722) disappeared more quickly in the presence of ferrous ions, suggesting that the addition of ferrous ions could speed up the corrosion of Fe^0 core (Fig. 5a and b). Consequently, some new diffraction peaks appeared. These new peaks matched well with the standard pattern of lepidocrocite (FeOOH; JCPDS, file no. 1-136), a corrosion product of the Fe^0 [32]. SEM observation revealed that the nanowires were broken up along with increasing reaction time and no well-defined nanowires was left after 2 h of reaction in the Fe(II)/Fe@Fe_2O_3/air system (Fig. 6a–d). We observed some nanosheets, which might be ascribed to the renascent FeOOH (Fig. 6e). We also investigated the effect of the renascent FeOOH on the simazine degradation and found that simazine could not be decomposed by FeOOH or Fe(II)/FeOOH (Fig. 7a), ruling out the contribution of in-situ generated FeOOH on the simazine removal in this study. To check the role of molecular oxygen on the aerobic simazine degradation process, we compared the removal efficiencies of simazine over

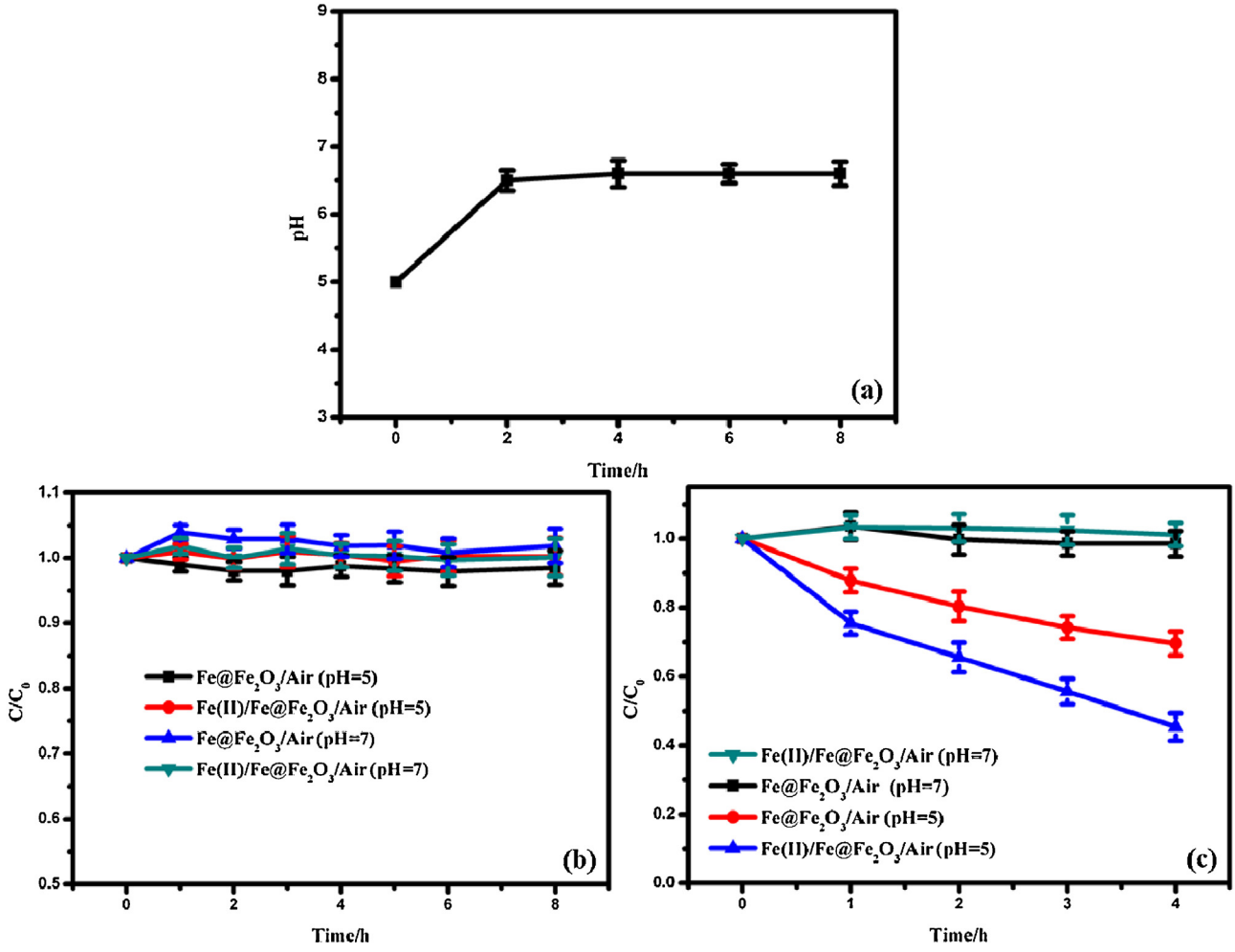

Fig. 3. (a) The changes of the pH value during the simazine removal in $Fe@Fe_2O_3$/air system at the initial pH of 5.0; (b) the aerobic removal curves of simazine with $Fe@Fe_2O_3$ and $Fe(II)/Fe@Fe_2O_3$ in the sodium acetate buffer (pH = 5.0) and piperazine-*N*,*N*′-bis(ethanesulfonic acid) buffer (pH = 7.0); and (c) The aerobic removal curves of 4-chlorophenol with $Fe@Fe_2O_3$ and $Fe(II)/Fe@Fe_2O_3$ in the sodium acetate buffer (pH = 5.0) and piperazine-*N*,*N*′-bis(ethanesulfonic acid) buffer (pH = 7.0).

$Fe@Fe_2O_3$ and $Fe(II)/Fe@Fe_2O_3$ under the different atmospheres (air or Ar). Simazine could be removed neither in the $Fe@Fe_2O_3$/Ar nor $Fe(II)/Fe@Fe_2O_3$/Ar systems (Fig. 7b), which can rule out the direct simazine reduction by Fe^0 core or ferrous ions. This comparison clearly revealed that the simazine removal in the $Fe@Fe_2O_3$/air and $Fe(II)/Fe@Fe_2O_3$/air systems involved molecular oxygen activation processes. The higher simazine removal efficiency in the $Fe(II)/Fe@Fe_2O_3$/air systems suggests that the addition

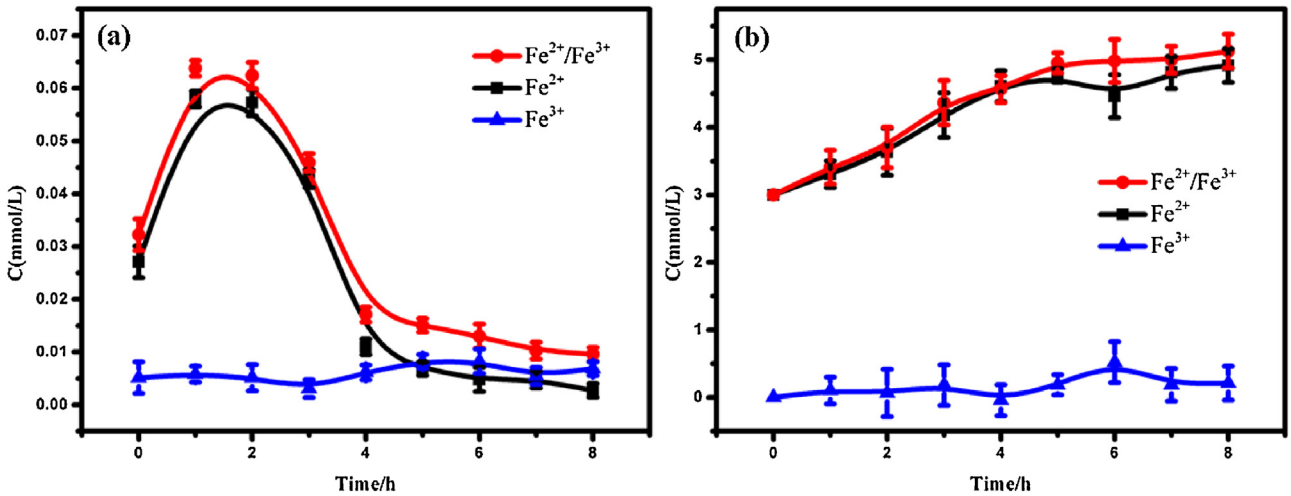

Fig. 4. The concentration of dissolved ferrous, ferric and total iron ions determined by 1,10-phenanthrolin method in different systems: (a) the $Fe@Fe_2O_3$/air system; and (b) the $Fe(II)/Fe@Fe_2O_3$/air system.

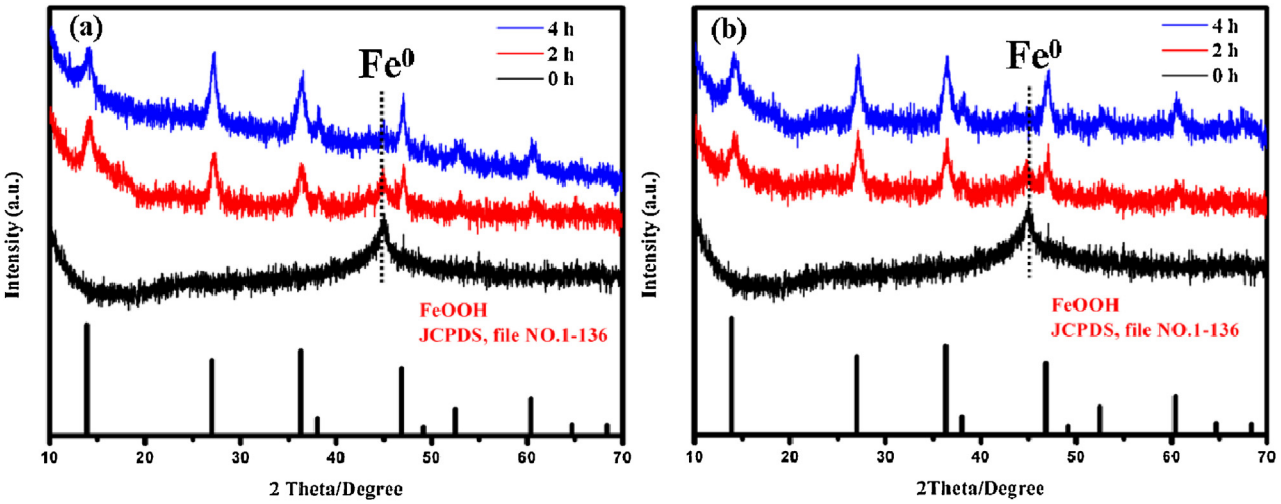

Fig. 5. XRD patterns of the Fe@Fe_2O_3/air nanowires before and after the removal process: (a) the Fe@Fe_2O_3/air system; and (b) the Fe(II)/Fe@Fe_2O_3/air system.

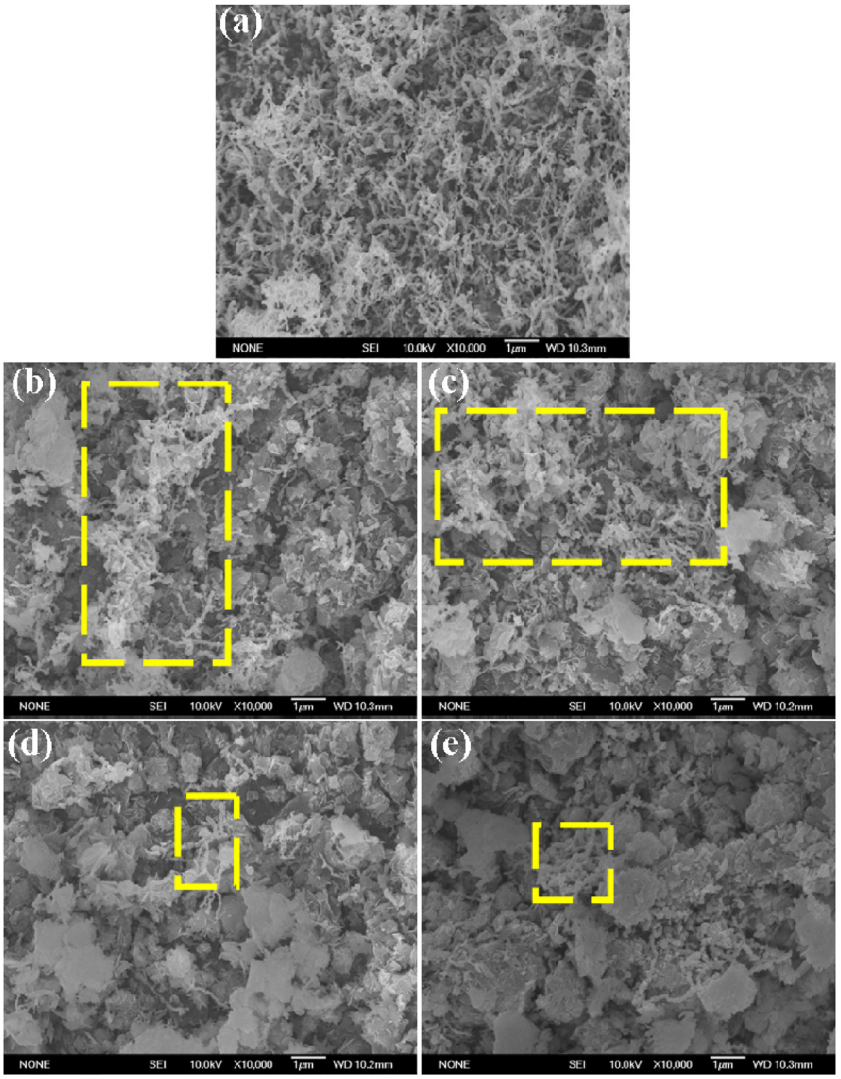

Fig. 6. SEM of the Fe@Fe_2O_3 nanowires before and after the simazine removal process: (a) the as-prepared Fe@Fe_2O_3 nanowires; (b) after 2 h and (c) after 4 h of reaction in the Fe@Fe_2O_3/air system; (d) after 2 h and (e) after 4 h of reaction in the Fe(II)/Fe@Fe_2O_3/air system.

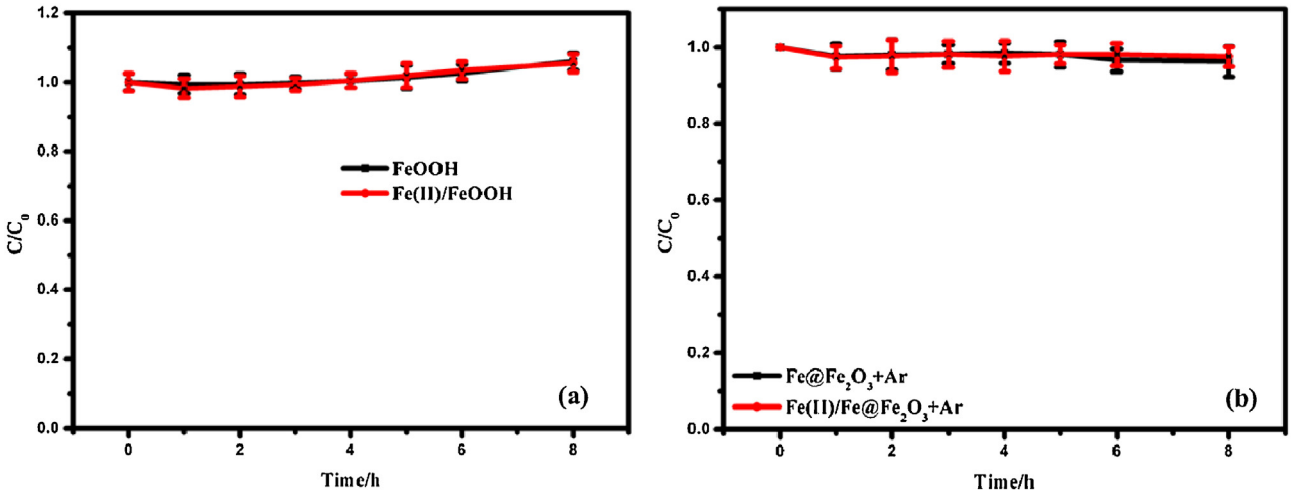

Fig. 7. (a) The aerobic removal curves of simazine with FeOOH and Fe(II)/FeOOH; and (b) The degradation curves of simazine over $Fe@Fe_2O_3$ and $Fe(II)/Fe@Fe_2O_3$ under Ar atmosphere.

of ferrous ions might promote the molecular oxygen activation process to generate more ROSs.

Our recent study revealed that two molecular oxygen activation pathways simultaneously governed the aerobic degradation of 4-chlorophenol with $Fe@Fe_2O_3$ nanowires, resulting in the interesting core–shell structure dependent reactivity of $Fe@Fe_2O_3$ nanowires [29]. Among the two pathways, one is the two-electron reduction of molecular oxygen to produce H_2O_2, which

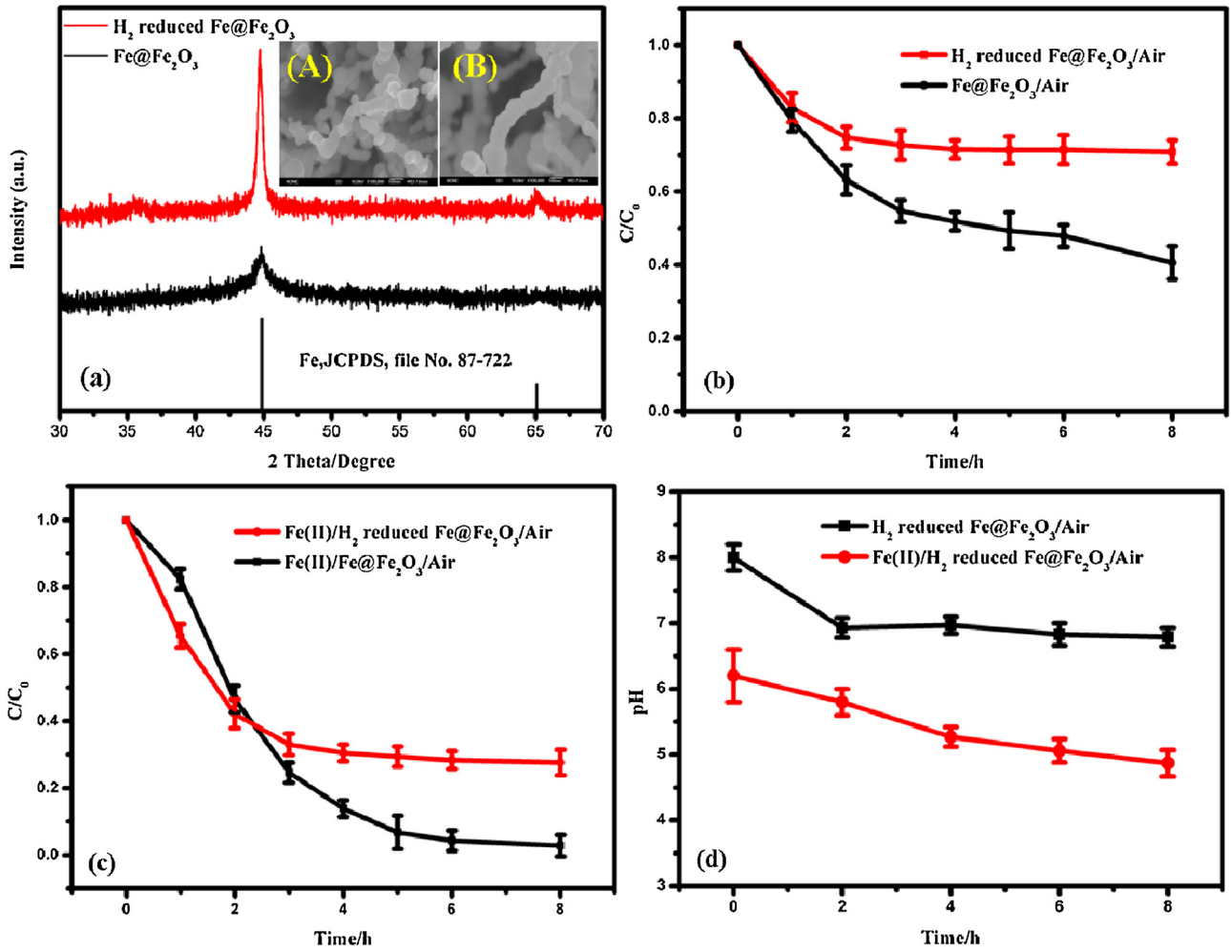

Fig. 8. (a) The XRD patterns and SEM images (inset) of the as-prepared $Fe@Fe_2O_3$ nanowires and the H_2 reduced $Fe@Fe_2O_3$; (b) The aerobic removal curves of simazine with $Fe@Fe_2O_3$ and H_2 reduced $Fe@Fe_2O_3$; (c) The aerobic removal curves of simazine with $Fe@Fe_2O_3$ and the H_2 reduced $Fe@Fe_2O_3$ in the presence of ferrous ions; and (d) The changes of the pH value during the simazine removal in H_2 reduced $Fe@Fe_2O_3$/air and $Fe(II)/H_2$ reduced $Fe@Fe_2O_3$/air systems.

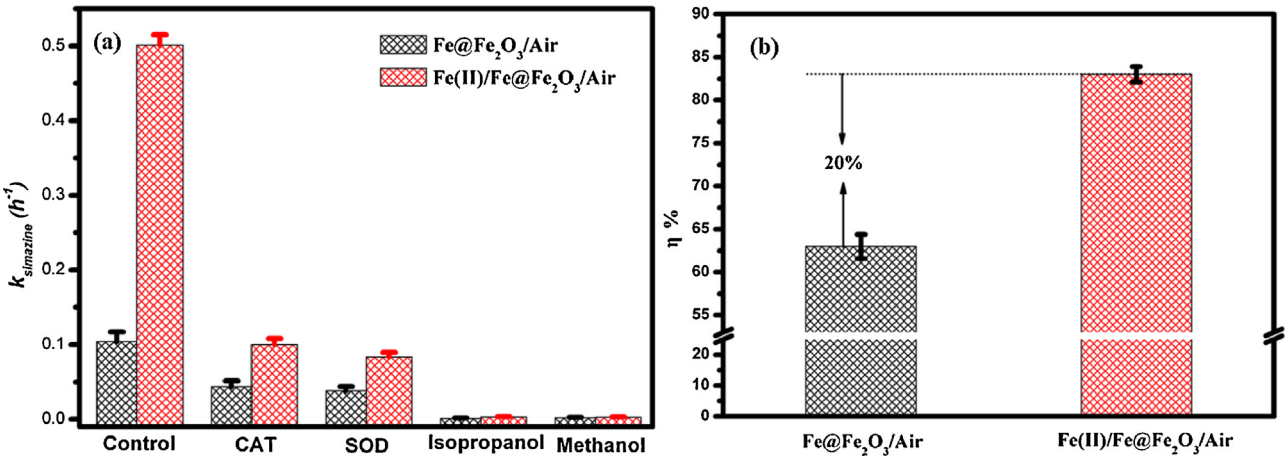

Fig. 9. (a) The apparent degradation constants for the aerobic removal of simazine in Fe@Fe_2O_3/air and Fe(II)/Fe@Fe_2O_3/air systems with different scavengers (CAT for H_2O_2, SOD for $\cdot O_2^-$, isopropanol and methanol for ·OH, respectively); and (b) The inhibitory ratio of simazine by Fe@Fe_2O_3/air and Fe(II)/Fe@Fe_2O_3/air with SOD for $\cdot O_2^-$.

is realized through the electron transfer from the Fe^0 core to the surface of iron oxide shell via the conduction band of iron oxide. The other is the single-electron reduction of molecular oxygen to superoxide anions by the surface bound ferrous ions ($\equiv Fe^{III}OFe^{II}OH/\equiv Fe^{II}OFe^{III}OH$). The generated superoxide anions would further react with protons and electrons to generate H_2O_2 [33]. All the generated H_2O_2 would then react with the dissolved and surface bound ferrous ions to produce hydroxyl radicals via Fenton reaction. The generation of hydroxyl radicals in the two systems was confirmed by the terephthalic acid fluorescence method (Fig. S1, Appendices A and B).

To verify the contribution of the surface bound ferrous ions to the aerobic degradation of simazine, we pretreated Fe@Fe_2O_3 with a mixture gas of 3% H_2 and 97% Ar at 400 °C for 1 h (H_2 reduced Fe@Fe_2O_3) to reduce the surface ferrous ions bound on the oxide shell [34], and then used the H_2 reduced Fe@Fe_2O_3 for the aerobic removal of simazine. XRD and SEM characterization revealed that hydrogen reduction could increase the crystallinity of metallic iron without changing the morphology of the nanowires (Fig. 8a). However, the removal efficiency of simazine over H_2 reduced Fe@Fe_2O_3 decreased remarkably no matter whether ferrous ions were added or not (Fig. 8b and c). We also monitored the pH values in these two H_2 reduced Fe@Fe_2O_3-containing systems and found the pH changes were almost the same as those of the Fe@Fe_2O_3-containing systems (2a and 8d), which could further rule out the contribution of pH change to the enhanced aerobic simazine degradation in the Fe(II)/Fe@Fe_2O_3/air system and also confirm the indispensable contribution of surface bound ferrous ions to molecular oxygen activation.

To clarify the origin of the enhanced aerobic simazine removal with Fe@Fe_2O_3 nanowires by extra ferrous ions, we therefore investigated the generation of ROSs in the Fe@Fe_2O_3/air and Fe(II)/Fe@Fe_2O_3/air systems with adding different kinds of scavengers (SOD for O_2^-, CAT for H_2O_2, iso-propanol and methanol for total ·OH) [19,35]. The aerobic simazine degradation was largely depressed by the addition of iso-propanol and methanol (Fig. 9a), revealing the major role of ·OH on the degradation of simazine. Interestingly, the simazine degradation efficiencies also decreased after adding SOD and CAT, suggesting that $\cdot O_2^-$ and H_2O_2 were also involved in the two systems. In order to further understand the role of $\cdot O_2^-$ during the simazine removal processes, we calculated the inhibitory efficiency (η) of SOD in both of these two systems through Eq. (1).

$$\eta\% = \left[\frac{(k_0 - k_t)}{k_0}\right] \times 100\% \quad (1)$$

where k_0 and k_t were, respectively, the apparent degradation constants in the absence or presence of SOD and we assumed that the $\cdot O_2^-$ could be completely trapped by excess SOD. We found that η was about 63% in the Fe@F_2O_3/air system, suggesting the single-electron reduction of molecular oxygen to generate O_2^- by surface bound ferrous ions is the major molecular oxygen activation pathway in the Fe@F_2O_3/air system (Fig. 9b). As expected, η increased to about 83% after adding ferrous ions, indicating that more $\cdot O_2^-$ was generated by the single-electron molecular oxygen activation to participate in the simazine degradation process in the Fe(II)/Fe@Fe_2O_3/air system. Obviously, the 20% of enhancement on the $\cdot O_2^-$ generation could not well explain about 400% of enhancement on the apparent simazine degradation constant after adding ferrous ions. Further investigation is essential to understand the reasons for the enhanced simazine degradation by more surface bound ferrous ions arisen from the extra ferrous ions in the Fe(II)/Fe@Fe_2O_3/air system. Therefore, we measured the amount of H_2O_2 generated via the two-electron transfer molecular oxygen reduction pathway in the Fe@F_2O_3/air and Fe(II)/Fe@Fe_2O_3/air systems by adding excess 2,2′-bipytridine (BPY), which is a strong ligand to complex ferrous ions to prevent their oxidation by hydrogen peroxide and oxygen [36,37]. As shown in Fig. 10, the presence of BPY could greatly inhibit the generation of H_2O_2 in these two systems, while the ratio of maximum concentration of hydrogen

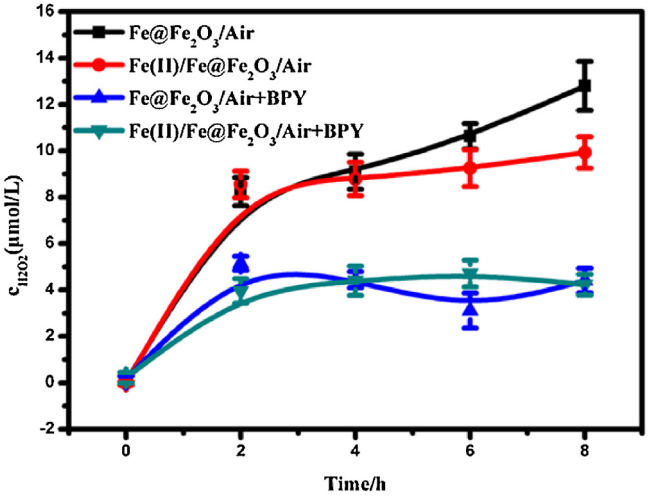

Fig. 10. The concentration of H_2O_2 generated in Fe@Fe_2O_3/air and Fe(II)/Fe@Fe_2O_3/air systems in the absence or presence of BPY.

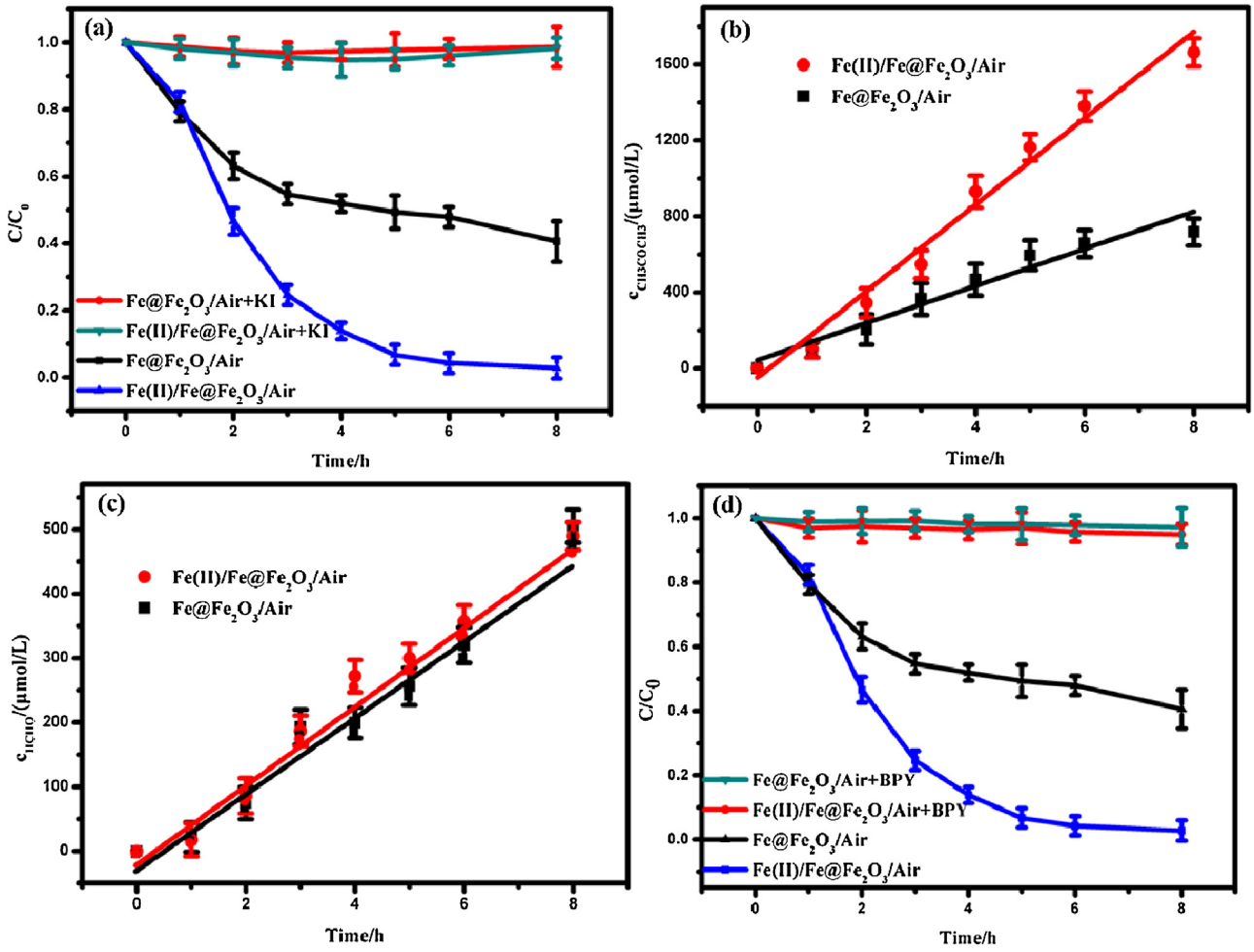

Fig. 11. (a) The aerobic removal curves of simazine by $Fe@Fe_2O_3$/air and $Fe(II)/Fe@Fe_2O_3$/air in the absence or presence of KI to capture the hydroxyl radical on the surface of $Fe@Fe_2O_3$; (b) $\cdot OH_{total}$ generation curves reflected by the oxidation of iso-propanol in the $Fe@Fe_2O_3$/air and $Fe(II)/Fe@Fe_2O_3$/air systems; (c) $\cdot OH_{free}$ generation curves reflected by the oxidation of methanol in the $Fe@Fe_2O_3$/air and $Fe(II)/Fe@Fe_2O_3$/air systems; and (d) The aerobic removal curves of simazine in different systems in the absence or presence of BPY.

peroxide in the presence of BPY was about 40% of that without adding BPY in the $Fe@Fe_2O_3$/air system, suggesting that about 60% of H_2O_2 was generated via the single-electron molecular oxygen activation by surface bound ferrous ions. This result matched very well with the aforementioned SOD inhibitory result. We noticed that in the absence of BPY the concentration of H_2O_2 generated in the $Fe(II)/Fe@Fe_2O_3$/air system was slightly lower than that in the $Fe@Fe_2O_3$/air system after 4 h, which might be attributed to more H_2O_2 decomposition by the extra ferrous ions and/or more $\cdot O_2^-$ consumption by the generated ferric ions via the Haber–Weiss reaction [38]. The lower aerobic simazine removal efficiency at the ferrous ions dosage of 5 mmol/L than that of 3 mmol/L might also be ascribed to $\cdot O_2^-$ consumption by excess ferric ions.

It is known that two kinds of hydroxyl radicals might be generated over heterogeneous catalysts [39]. To check the types of hydroxyl radicals generated in the $Fe@Fe_2O_3$/air system, we first employed KI as the scavenger to probe the generation of hydroxyl radicals bound to the surface of catalyst ($\cdot OH_{bound}$) [40]. It was interesting to find that the addition of excess KI resulted in a complete inhibition of simazine degradation in the two systems (Fig. 11a), indicating that surface hydroxyl radicals played a vital role on the simazine removal in the two systems. Both methanol and 2-propanol were usually used to capture the hydroxyl radicals in zero valent iron system [19,20]. As methanol has low affinity to oxide surfaces, it can only be oxidized by hydroxyl radicals in the bulk solution [20]. We therefore chose the oxidation of methanol and isopropanol to probe the amount of hydroxyl radical in the solution ($\cdot OH_{sol}$) and total hydroxyl radical ($\cdot OH_{total}$) generated, respectively. The concentrations of $\cdot OH_{total}$ and $\cdot OH_{sol}$ in both of the two systems increased linearly and the generation curves of $\cdot OH_{total}$ and $\cdot OH_{sol}$ obeyed zero-order kinetics equations (Fig. 11b and c). The ratio of $\cdot OH_{total}$ generation constants of $Fe(II)/Fe@Fe_2O_3$/air to $Fe@Fe_2O_3$/air systems was 2.33, but only 1.03 for $\cdot OH_{sol}$. This ratio difference might be attributed to more surface bound hydroxyl radicals generated in the $Fe(II)/Fe@Fe_2O_3$/air system. Because hydroxyl radicals are generated through Fenton reaction in the two systems, it is reasonable for us to correlate the more surface hydroxyl radicals generated in the $Fe(II)/Fe@Fe_2O_3$/air system to its more surface bound ferrous ions. As aforementioned, more surface bound ferrous ions in the $Fe(II)/Fe@Fe_2O_3$/air system could activate molecular oxygen via the single-electron transfer pathway to produce only more than 20% of $\cdot O_2^-$ and H_2O_2 dissolved in the solution than those in the $Fe@Fe_2O_3$/air system according to SOD and BPY inhibitory experimental results. Obviously, the enhancement of O_2^- and H_2O_2 dissolved in the solution was far less than those of final simazine degradation efficiency and $\cdot OH_{total}$ amount in the $Fe(II)/Fe@Fe_2O_3$/air system. Therefore, we hypothesize that more $\cdot O_2^-$ and H_2O_2 bound to the surface of $Fe@Fe_2O_3$ nanowires might be generated by more surface bound ferrous ions in the $Fe(II)/Fe@Fe_2O_3$/air system. These surface bound H_2O_2 would

react with surface bound and/or dissolved ferrous ions to produce $\cdot OH_{bound}$.

To validate the above opinion, we utilized 2,2′-bipytridine (BPY) to complex both dissolved and surface bound ferrous ions to inhibit the Fenton reaction. Similar to the case of iso-propanol, the addition of BPY could almost completely inhibit the aerobic degradation of simazine (Fig. 11d). Although H_2O_2 could still be generated via the two-electron transfer pathway by the Fe^0 in the presence of BPY, it was hardly decomposed to generate hydroxyl radicals to degrade simazine, which could well explain the complete inhibitory effect of BPY on the aerobic degradation of simazine. So we conclude that these surface bound hydroxyl radicals are generated from the surface bound ferrous ions.

On the basis of the above results and analyses, we proposed a possible surface bound hydroxyl radical generation mechanism during the aerobic degradation of simazine over Fe@Fe_2O_3 nanowires (Scheme 1a). First, molecular oxygen adsorbed on the surface of iron oxide could be reduced to surface bound hydrogen peroxide via the two-electron molecular oxygen activation pathway by the outward electron transfer from iron core to the iron oxide shell surface. Meanwhile, the surface bound ferrous ions would reduce molecular oxygen through the single-electron transfer pathway to generate surface bound superoxide anions, which would further react with protons and electrons to produce surface bound hydrogen peroxide. According to the H_2O_2 detection results, the contribution of the sequential single-electron transfer pathway on the H_2O_2 generation was more than 60%, higher than that of the two-electron molecular oxygen activation pathway. Subsequently, all the surface bound hydrogen peroxide would react with surface bound and/or dissolved ferrous ions to produce $\cdot OH_{bound}$. Meanwhile, a small fraction of the surface bound ROSs would diffuse into the solution as free ROSs. Therefore, the

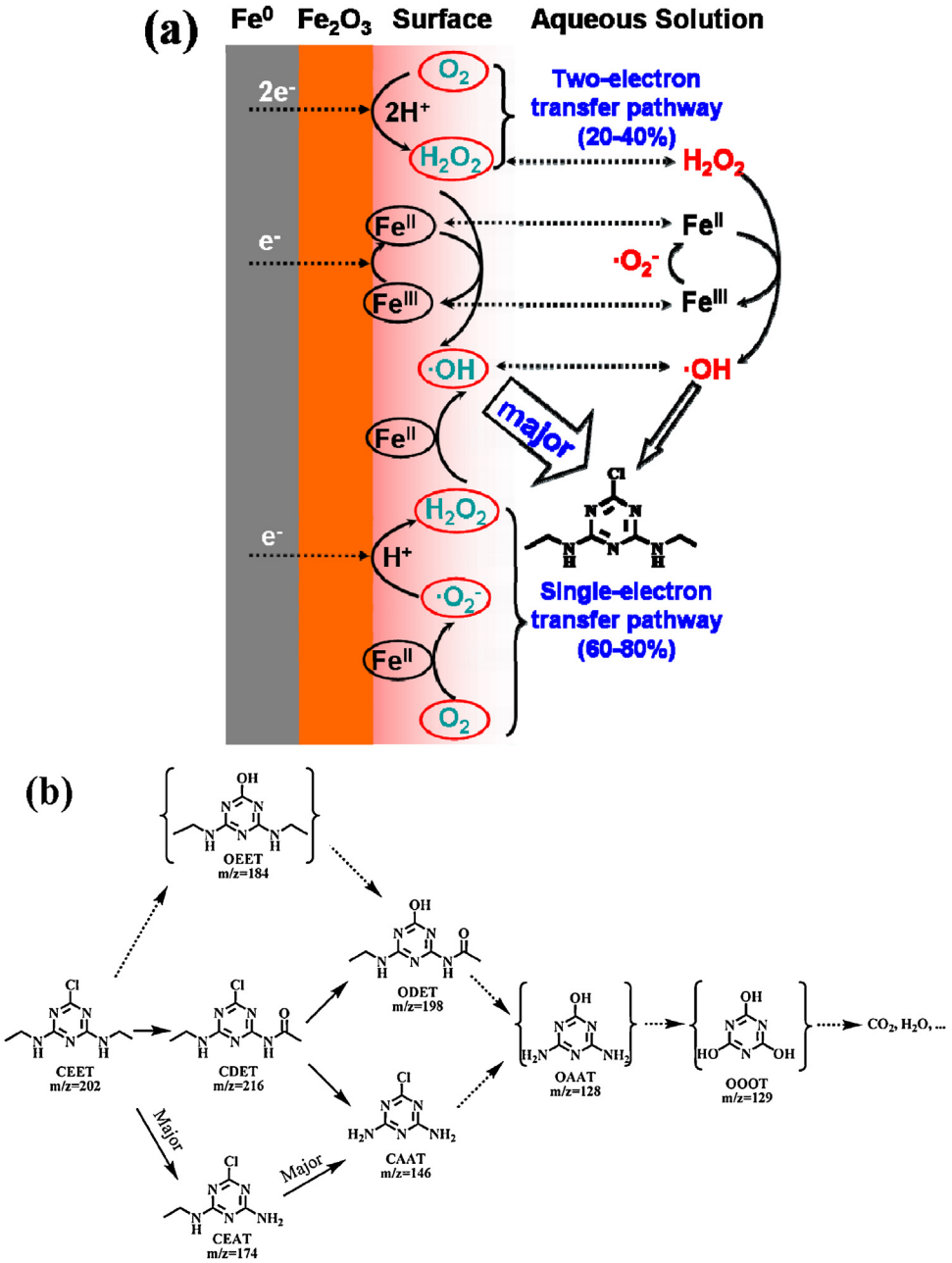

Scheme 1. (a) The possible surface bound hydroxyl radical generation mechanism during the aerobic degradation of simazine over Fe@Fe_2O_3 nanowires; (b) The proposed simazine degradation mechanism in the Fe@Fe_2O_3/air system.

ferrous ions enhanced aerobic degradation of simazine over Fe@Fe_2O_3 nanowires could be explained as follows. The addition of ferrous ions in the Fe@Fe_2O_3/air system could not only maintain enough dissolved ferrous ions for the fast decomposition of H_2O_2 and speed up the electrons transfer from iron cores to iron oxide shells for the subsequent two electron reduction molecular oxygen activation on the surface of Fe@Fe_2O_3 nanowires, but also enhance the single-electron reduction molecular oxygen activation by providing more surface bound ferrous ions on the iron oxide shell. Subsequently, these more surface bound ferrous ions would react with surface bound hydrogen peroxide to produce more surface hydroxyl radicals bound to Fe@Fe_2O_3 nanowires, which mainly contribute to the enhanced simazine degradation observed in this study.

We detected the intermediates of simzaine degradation with LC–MS and GC–MS and found no significant difference between the intermediates in the two systems. The found intermediates include 6-chloro-2-acetamido-4-(ethylamino)-1,3,5-triazine (CDET), 6-hydroxy-2-acetamido-4-(ethylamino)-1,3,5-triazine (ODET), 6-chloro-*N*-ethyl-[1,3,5] triazine-2,4-diamine (CEAT), 6-chloro-[1,3,5]triazine-2, 4-diamine (CAAT). On the basis of these intermediates, we tentatively proposed the aerobic degradation pathway of simazine over Fe@Fe_2O_3 nanowires as follows (Scheme 1b). The simazine degradation involved alkylic oxidation, dealkylation and dechlorination pathway. The first and major step was the dealkylation from the C–N bond of the ethylamino side chain to generate CEAT because the electron-rich positions were more susceptible to be attacked by the electrophilic ·OH. The produced CEAT was subsequently decomposed by the attack of ·OH to generate CAAT. Meanwhile, the secondary C of ethylamino side chain was oxidized to carbonyl group by ·OH to form CDET. Dechlorination-hydroxylation would also take place via the ·OH attack on the C–Cl bond of *s*-triazine ring to produce ODET. Unfortunately, we did not found out other intermediates like cyanuric acid (1, 3, 5-triazine-2,4,6-triol, OAAT) in the system, which may be caused by the low conversion rate of CAAT to OAAT.

4. Conclusions

In summary, we have demonstrated that the extra ferrous ions could promote the aerobic simazine removal efficiency of Fe@Fe_2O_3 nanowires. The enhancement was realized by maintaining enough dissolved ferrous ions and enhancing the single-electron reduction molecular oxygen activation via providing more surface bound ferrous ions on the iron oxide shell. We found that more surface bound ferrous ions could also produce more surface hydroxyl radicals for the enhanced simazine degradation. The 2,2′-bipytridine inhibition and reactive oxygen species detection experimental results revealed that the contribution of single-electron molecular oxygen activation via surface bound ferrous ions to reactive oxygen species production was more than 60%, higher than that of two-electron molecular oxygen activation pathway. These interesting findings could provide new insight on nanoscale zero valent iron induced molecular oxygen activation and its aerobic removal of organic pollutants at circumneutral pH.

Acknowledgments

This work was supported by National Science Foundation of China (Grants 21073069, 91023010, 21173093, and 21177048) and Self-Determined Research Funds of CCNU from the Colleges Basic Research and Operation of MOE (CCNU11C01002). Key Project of Natural Science Foundation of Hubei Province (Grant 2013CFA114), and Excellent Doctorial Dissertation Cultivation Grant from central China Normal University (Grant 2013YBYB59).

Appendix A. Supplementary data

Supplementary data associated with this article can be found, in the online version, at http://dx.doi.org/10.1016/j.apcatb.2013.11.034.

References

[1] A.S. Gunasekara, J. Troiano, K.S. Goh, R.S. Tjeerdema, Rev. Environ. Contam. Toxicol. 189 (2007) 1–23.
[2] M.T. Strandberg, J.J. Scott-Fordsmand, Sci. Total Environ. 296 (2002) 117–137.
[3] Environmental Protection Agency. Federal Register, Wednesday, 26 June, Part VII, 40 CFR Parts 152 and 156, 1996.
[4] R.O. López-Flores, X.D. Quintana, V. Salvadó, M. Hidalgo, L. Sala, R. Moreno-Amich, Water Res. 37 (2003) 3034–3046.
[5] K. Vandecasteele, I. Gaus, W. Debreuck, K. Walraevens, Anal. Chem. 72 (2000) 3093–3101.
[6] C.G. Cogger, P.R. Bristow, J.D. Stark, L.W. Getzin, M. Montgomery, J. Environ. Qual. 27 (1998) 543–550.
[7] J.R. Vogel, S.M. Michael, P.D. Capel, J. Environ. Qual. 37 (2008) 1101–1115.
[8] M. Cruz-Guzmán, R. Celis, M.C. Hermosín, J. Cornejo, Environ. Sci. Technol. 38 (2003) 180–186.
[9] E.C. Catalkaya, F. Kargi, J. Hazard. Mater. 168 (2009) 688–694.
[10] W. Chu, Y.F. Rao, W.Y. Hui, J. Agric. Food Chem. 57 (2009) 6944–6949.
[11] F.J. Beltrán, J.F. García-Araya, V. Navarrete, F.J. Rivas, Ind. Eng. Chem. Res. 41 (2002) 1723–1732.
[12] J.S.d. Santos, V. Palaretti, A.L.d. Faria, E.J. Crevelin, L.A.B.d. Moraes, M.d.D. Assis, Appl. Catal., A 408 (2011) 163–170.
[13] S. Hippeli, E.F. Elstner, FEBS Lett. 443 (1999) 1–7.
[14] B.F. Minaev, Int. J. Quantum Chem. 17 (1980) 367–374.
[15] C. Long, D.R. Kearns, J. Chem. Phys. 59 (1973) 5729–5736.
[16] C. Noradoun, M.D. Engelmann, M. McLaughlin, R. Hutcheson, K. Breen, A. Paszczynski, I.F. Cheng, Ind. Eng. Chem. Res. 42 (2003) 5024–5030.
[17] S.H. Joo, A.J. Feitz, T.D. Waite, Environ. Sci. Technol. 38 (2004) 2242–2247.
[18] O.X. Leupin, S.J. Hug, Water Res. 39 (2005) 1729–1740.
[19] S.H. Joo, A.J. Feitz, D.L. Sedlak, T.D. Waite, Environ. Sci. Technol. 39 (2005) 1263–1268.
[20] C.R. Keenan, D.L. Sedlak, Environ. Sci. Technol. 42 (2008) 1262–1267.
[21] L.R. Lu, Z.H. Ai, F.L. Jia, L.Z. Zhang, Cryst. Growth Des. 7 (2007) 459–464.
[22] Z.H. Ai, L.R. Lu, J.P. Li, L.Z. Zhang, J.R. Qiu, M.H. Wu, J. Phys. Chem. C 111 (2007) 4087–4093.
[23] Z.H. Ai, L.R. Lu, J.P. Li, L.Z. Zhang, J.R. Qiu, M.H. Wu, J. Phys. Chem. C 111 (2007) 7430–7436.
[24] Z.H. Ai, T. Mei, J. Liu, J.P. Li, F.L. Jia, L.Z. Zhang, J.R. Qiu, J. Phys. Chem. C 111 (2007) 14799–14803.
[25] T. Luo, Z.H. Ai, L.Z. Zhang, J. Phys. Chem. C 112 (2008) 8675–8681.
[26] Z.H. Ai, Y.N. Wang, M. Xiao, L.Z. Zhang, J.R. Qiu, J. Phys. Chem. C 112 (2008) 9847–9853.
[27] Y.L. Chen, Z.H. Ai, L.Z. Zhang, J. Hazard. Mater. 235-236 (2012) 92–100.
[28] Z.H. Ai, Y. Cheng, L.Z. Zhang, J.R. Qiu, Environ. Sci. Technol. 42 (2008) 6955–6960.
[29] Z.H. Ai, Z.T. Gao, L.Z. Zhang, W.W. He, J.J. Yin, Environ. Sci. Technol. 47 (2013) 5344–5352.
[30] H. Tamura, K. Goto, T. Yotsuyanagi, M. Nagayama, Talanta 21 (1974) 314–318.
[31] R. Schick, I. Strasser, H.H. Stabel, Water Res. 31 (1997) 1371–1378.
[32] Y.H. Huang, T.C. Zhang, Water Res. 39 (2005) 1751–1760.
[33] G.D. Fang, D.M. Zhou, D.D. Dionysiou, J. Hazard. Mater. 250-251 (2013) 68–75.
[34] J. Zieliński, I. Zglinicka, L. Znak, Z. Kaszkur, Appl. Catal., A 381 (2010) 191–196.
[35] S.L. Atalla, L.H. Toledo-Pereyra, G.H. Mackenzie, J.P. Cederna, Transplantation 40 (1985) 584–589.
[36] I.A. Katsoyiannis, T. Ruettimann, S.J. Hug, Environ. Sci. Technol. 42 (2008) 7424–7430.
[37] G.D. Fang, D.D. Dionysiou, S.R. Al-Abed, D.M. Zhou, Appl. Catal., B 129 (2013) 325–332.
[38] W.H. Koppenol, Redox Rep. 6 (2001) 229–234.
[39] L.J. Xu, J.L. Wang, Environ. Sci. Technol. 46 (2012) 10145–10153.
[40] S.T. Martin, A.T. Lee, M.R. Hoffmann, Environ. Sci. Technol. 29 (1995) 2567–2573.